The Endothelial Glycocalyx is Hydrodynamically Relevant in Arterioles throughout the Cardiac Cycle

Michele D. Savery and Edward R. Damiano
Department of Biomedical Engineering, Boston University, Boston, Massachusetts

ABSTRACT The existence of a hydrodynamically relevant endothelial glycocalyx of ~0.5 μm in thickness is well established in capillaries and venules in vivo. Since the glycocalyx is likely to have implications for broad areas of vascular physiology and pathophysiology, including endothelial-cell mechanotransduction, vascular permeability, and atherosclerosis, it is necessary to determine the extent to which the glycocalyx is present on arteriolar endothelium. We applied microviscometric analysis to data obtained using microparticle image velocimetry in cremaster-muscle arterioles of wild-type mice. Due to the pulsatile nature of the flow regimes in arterioles, data acquisition was triggered with the electrocardiogram at specific time points in the cardiac cycle. Results show the existence of a hydrodynamically relevant glycocalyx having a mean thickness of 0.38 μm in arterioles ~20–70 μm in diameter ($n = 20$), which is ~0.13 μm thinner ($p = 0.03$) than that found previously in venules having a similar diameter range and under similar hemodynamic conditions. Results from data obtained at multiple time points in the cardiac cycle show that the glycocalyx remains hydrodynamically relevant in arterioles with statistically insignificant changes in mean thickness throughout the cardiac cycle, despite the inherent unsteadiness of the flow regimes in these microvessels. These results provide direct in vivo confirmation of the existence of a hydrodynamically relevant surface glycocalyx that essentially eliminates fluid shear stress on arteriolar endothelium throughout the entire cardiac cycle.

INTRODUCTION

Much attention has recently been focused on the role of the endothelial-cell glycocalyx in a variety of processes in cardiovascular physiology and pathophysiology, including inflammation, microvascular permeability, endothelial-cell mechanotransduction, atherosclerosis, and diabetes (1–4). The fact that the native endothelial glycocalyx in vivo not only excludes macromolecules and flowing red blood cells from near-wall regions of microvessels <15 μm in diameter (5–7), but also retards plasma flow through these same regions of venules and eliminates fluid shear stress on the surface of venular endothelium, has now been well established (8–11). It has not been demonstrated, however, if the endothelial glycocalyx is indeed ubiquitous throughout the microcirculation in vivo or if it is preferential to small microvessels and postcapillary venules. In particular, the hydrodynamical relevance of the endothelial glycocalyx in arterioles >15 μm in diameter has not been investigated in vivo. Furthermore, the presence of cardiac-induced pulsatility in arterioles, which is largely absent in postcapillary venules due to dampening effects throughout the capillary bed, may cause periodic perturbations in the glycocalyx throughout the cardiac cycle, which could influence the hydrodynamic environment near the endothelium. The differing hemodynamic environments between arterioles and venules may influence or even determine the extent to which the glycocalyx appears on arterial versus venular endothelium, which may in turn have important implications for endothelial mechanotransduction, angiogenesis, and atherosclerosis.

From μ-PIV data of the instantaneous speeds and radial positions of fluorescent microspheres (~0.5-μm diameter) traveling in an optical section through the median plane of venules, Damiano and co-workers (9–11) were able to extract velocity profiles over the cross section of venules ~20–100 μm in diameter. With the assumption that blood flow in microvessels >20 μm in diameter can be well approximated by a homogeneous, continuous linearly viscous fluid with spatially variable viscosity (9,10,12), the conservation of linear momentum and the constitutive equation for a linearly viscous fluid were used to estimate radial distributions in viscosity, shear rate, and shear stress and to probe the existence of a hydrodynamically relevant glycocalyx on the luminal surface of venules in vivo before and after light-dye and enzymatic treatments to degrade the glycocalyx. In addition, this approach, which Long et al. (10) termed ''microviscometric analysis,'' allowed for accurate estimates of pressure gradient and relative apparent viscosity in vivo. The effectiveness of microviscometry was validated in smooth cylindrical glass tubes (~30–80 μm in diameter) perfused with red cells suspended in plasma and in blood-perfused postcapillary venules in vivo (~20–60 μm in diameter) before and after isovolemic hemodilution (10).

Using microviscometry, together with a detailed three-dimensional analysis of the fluid dynamics around the microsphere and throughout the glycocalyx (13), Damiano and co-workers were able to show that the only possible velocity distribution within the glycocalyx that was consistent with the μ-PIV data had to be highly nonlinear and therefore indicative of a region near the vessel wall that significantly

Submitted January 22, 2008, and accepted for publication March 28, 2008.

Address reprint requests to Edward Damiano, Tel.: 617-353-9493; E-mail: edamiano@bu.edu.

Editor: Denis Wirtz.

0006-3495/08/08/1439/09 $2.00

doi: 10.1529/biophysj.108.128975

retards plasma flow (8–11). They showed that in mouse cremaster-muscle venules ~20–100 μm in diameter, this region extended ~0.5 μm from the vessel wall in control vessels, and was termed the ''effective hydrodynamically relevant thickness'' of the glycocalyx, where this quantity is understood to represent an average value that is characteristic of an inherently heterogeneous endothelial glycocalyx. After light-dye treatment to degrade the glycocalyx, the hydrodynamically relevant thickness was reduced to ~0.2 μm (9), whereas it was essentially absent after enzymatic digestion with hyaluronidase (11).

The main technical challenge in applying microviscometric analysis to arteriolar blood flow arises as a result of the flow pulsatility present in these vessels (14,15). To extract data from the same instantaneous velocity profile, we exploit the periodicity in the flow regime in these vessels and synchronize μ-PIV data acquisition with the animal's electrocardiogram (ECG). To do this, we adapt some of the methods developed by Tangelder et al. (14), in which the translational speeds of fluorescently-labeled platelets were tracked in arterioles in vivo and recorded on video tape. Rather than using platelets, which are too large to provide the spatial resolution necessary to accurately extract the velocity distribution through the plasma-rich zone near the vessel wall, we use neutrally buoyant fluorescently labeled polystyrene microspheres ~0.5-μm in diameter. As shown below, with a simple generalization of microviscometric analysis, all of the methods that we have developed to study microvascular hemodynamics in venules (8–10,13) can be applied in a straightforward manner to arterioles.

Considerations and methods for generalizing our microviscometric method to the analysis of hemodynamics in arterioles are detailed below. This generalized analysis is used to estimate the effective hydrodynamically relevant thickness of the endothelial glycocalyx in arterioles (~20–70 μm in diameter) before and after hyaluronidase treatment to degrade the layer. We further examine the influence of flow pulsatility on the hydrodynamically relevant glycocalyx thickness by comparing results obtained from μ-PIV data acquired from the same arteriole at four distinct time points in the cardiac cycle.

MICROVISCOMETRIC ANALYSIS OF ARTERIOLAR BLOOD FLOW

The governing equations used in microviscometry were derived for steady, axisymmetric, parallel flows in a cylindrical tube (9,10). However, these conditions can be relaxed to allow the approach to extend to unsteady flow regimes. For the case of an unsteady, instantaneously fully developed, axisymmetric parallel flow of an incompressible continuum fluid in a cylindrical tube of radius R, the only nonvanishing component of the deviatoric stress tensor, written in terms of the cylindrical coordinates (r, θ, z), is the shear stress component, τ_{rz}. Furthermore, from the radial momentum equation, the axial component of the pressure gradient, $\partial p/\partial z$, is a function only of time. Consequently, the axial momentum equation reduces to

$$\rho\frac{\partial v_z}{\partial t}-\frac{1}{r}\frac{\partial}{\partial r}(r\tau_{rz})=\frac{\partial p}{\partial z}=\text{func}(t)\ \text{only},\quad 0<r<R, \tag{1}$$

where ρ is the fluid density and $v_z(r, t)$ is the instantaneous axial velocity component of the fluid. Integrating twice with respect to r provides

$$\tau_{rz}=\frac{r}{2}\frac{\partial p}{\partial z}+\frac{\rho}{2\pi r}\frac{\partial q}{\partial t},\quad 0<r<R, \tag{2}$$

where

$$q(r,t)=2\pi\int_0^r v_z(\tilde{r},t)\tilde{r}\,d\tilde{r},\quad 0<r<R, \tag{3}$$

is the instantaneous volume flow rate through the circular cross-sectional area that is of radius r and is centered along the tube axis.

The importance of the inertial term can be readily ascertained by nondimensionalizing Eq. 2. If the radial and axial coordinates are nondimensionalized with respect to the tube radius, R, and p and τ_{rz} are nondimensionalized with the same characteristic pressure, $f\,\mu_p$, where μ_p is the dynamic viscosity of blood plasma and f is the characteristic forcing frequency (in Hz) of the pressure gradient, then Eq. 2 takes the dimensionless form

$$\tau^*_{rz}=\frac{r^*}{2}\frac{\partial p^*}{\partial z^*}+\frac{St}{r^*}\frac{\partial q^*}{\partial t^*},\quad 0<r^*<1, \tag{4}$$

where an asterisk denotes a nondimensional variable. In Eq. 4, the dimensionless volumetric flow rate $q^* = q/(R^3 f)$ and $St = \rho R^2 f/\mu_p$ is the Stokes number, which characterizes the ratio of unsteady inertial forces to viscous forces. If τ^*_{rz}, $\partial p^*/\partial z^*$, and $\partial q^*/\partial t^*$ are all of the same order of magnitude, then the relative importance of the inertial term in Eq. 4 can be assessed solely by considering the magnitude of the Stokes number. For the range of arteriolar diameters that we consider in this study, $7\times10^{-4} < St < 9\times10^{-3}$, assuming a maximum heart rate of ~500 beats/min (BPM). Thus, it is reasonable to neglect unsteady inertial forces in these vessels and to take $St = 0$. In this case, viscous forces and pressure-gradient forces are instantaneously in balance at any moment in the cardiac cycle, which implies that microviscometric analysis can be applied instantaneously at any moment in the cardiac cycle. Accordingly, we are justified in generalizing the steady-state microviscometric analysis of Damiano et al. (9), to obtain the unsteady viscosity distribution, shear stress distribution, and pressure gradient given, respectively, by

$$\frac{\mu(r,t)}{\mu_p}=\frac{r}{R}\frac{(\partial v_z/\partial r)|_{r=R}}{\partial v_z/\partial r}=\frac{r}{R}\frac{\dot{\gamma}(R,t)}{\dot{\gamma}(r,t)},\quad 0<r<R, \tag{5}$$

$$\tau_{rz}(r,t)=\mu(r,t)\dot{\gamma}(r,t)=\mu_p\frac{r}{R}\dot{\gamma}(R,t),\quad 0<r<R, \tag{6}$$

and

$$\frac{\partial p}{\partial z} = \frac{2\mu_p}{R}\dot{\gamma}(R,t), \tag{7}$$

where the shear rate and axial velocity profile are kinematically related according to $\partial v_z/\partial r = \dot{\gamma}(r,t)$.

These results can readily be applied to straight cylindrical sections of glycocalyx-lined microvessels by simply substituting for the tube radius, R, in Eqs. 5–7 the radial coordinate location, a, of the blood–glycocalyx interface. This is described in more detail for the case of steadily perfused glycocalyx-lined microvessels in Damiano et al. (9).

METHODS

Intravital experiments

All animal experiments were conducted under a protocol approved by the Boston University Institutional Animal Care and Use Committee (Protocol #2474). Wild-type male mice (C57Bl/6) were obtained from Charles River Labs (Wilmington, MA). All mice appeared healthy, were between 8 and 20 weeks of age, and weighed ~25–30 grams. Each mouse was placed in an anesthetic induction chamber for ~2 min, where 3% isoflurane mixed with oxygen was delivered at a flow rate of 500 cc/min through an anesthesia machine (Model 100 Vaporizer, SurgiVet, Waukesha, WI). After losing its righting reflex and remaining immobile in the chamber for ~1 min, the mouse was then removed to a heated surgical platform and intubated with 1.5% pure oxygen. Anesthesia was maintained through endotracheal intubation. After intubation, the isoflurane concentration was reduced to 1.5–2.0% throughout the experiment. Breathing rate and tidal volume were regulated based on body mass with an automated ventilator (Inspira ASV Pump, Harvard Apparatus, Holliston, MA). A carotid cannula was used for administration of microsphere solution, enzyme treatment, and P-selectin antibody (RB40.34, BD Biosciences, Madison, WI).

The cremaster muscle was prepared for intravital microscopy as described in Ley et al. (16). Briefly, the cremaster muscle was exteriorized, pinned to the stage, and superfused with thermocontrolled bicarbonate-buffered saline equilibrated with 5% CO_2 in N_2. This procedure was completed in ~20 min. The ECG was recorded (PowerLab 4/30, AD Instruments, Colorado Springs, CO) for heart rate monitoring and to trigger the stroboscopic flash at specific time points in the cardiac cycle. Experiments were terminated if the heart rate dropped below 300 BPM. Enzymatic treatment of the endothelial glycocalyx followed the method described by Henry and Duling (6). The mouse received a single bolus containing 100 U *Streptomyces* hyaluronidase (Sigma Chemical, St. Louis, MO) in PBS through the carotid cannula for a blood concentration of ~93 U/mL. The enzyme was allowed to circulate through the blood stream for ~1 h before data were collected.

Microparticle image velocimetry

Intravital microscopic observations were made on a Zeiss microscope (Axioskop II, Carl Zeiss, Thornwood, NY) with a 63× saline immersion objective (NA 1.0), focused on the midsagittal plane of the vessel. The midsagittal plane was defined as corresponding to the focal plane at which the contrast of the edge of the intraluminal wall reversed (17). Microparticle image velocimetry (μ-PIV) was performed using a variation on a previously described method (8). Briefly, Fluoresbrite YG microspheres (0.538 ± 0.01 μm, ρ = 1.05 g/cm^3, Polysciences, Warrington, Pennsylvania) or Polychromatic red microspheres (0.513 ± 0.015 μm, ρ = 1.05 g/cm^3, Polysciences) were visualized using stroboscopic double-flash (4–9 ms apart, DPS-1 Video, Rapp OptoElectronic, Hamburg, Germany) epiillumination. A small volume (<0.05 ml) of fluorescent microspheres was slowly injected through the carotid cannulus until 10–20 microspheres per second passed through the vessel. Recordings were then made with a CCD camera (SensiCam QE, Cooke, Auburn Hills, MI) connected to a G5 Power Mac (Apple Computer, Cupertino, CA). A Dualview beam splitter (Optical Insights, Tucson, AZ) separated infrared transillumination from the fluorescent microsphere image, allowing for simultaneous acquisition of the vessel wall and the particle tracers. The camera and stroboscopic flash were triggered by the ECG. Images were captured and processed with IPLab software (BD Biosciences). A minimum of 300 frames were captured for each data set. The flash-time interval for μ-PIV recordings was chosen such that two images for a given microsphere were 3–10 μm apart and appeared as a double exposure on the same digital image.

Data from each arteriole were collected 10 ms after peak systole in the cardiac cycle. In a subset of arterioles, five sets of data were recorded, with each data set being collected at a single time point in the cardiac cycle. The first data set (A) was recorded 10 ms after peak systole. The following three data sets (B–D) were each collected at a specific time point in the cardiac cycle such that the four data sets were equally spaced throughout the cycle. A final data set (A′) was collected at the same time point in the cardiac cycle as the first (A). The total time required to collect these five data sets was typically ~10–15 min.

Microviscometric analysis

Images were analyzed with the public domain software, ImageJ (http://rsb.info.nih.gov/ij/), as previously described (8). The distance between the two images of the doubly exposed microsphere and the shortest distance between the microsphere center and the vessel wall were measured for at least 40 microspheres in each microvessel. Since not all of the recorded microspheres travel in the midsagittal plane, only the fastest microspheres at a given measured radial location were considered (where it is understood that a microsphere in the midsagittal plane travels faster than any other microsphere at that measured radial location) using a previously described monotonic filter (8,9). Only filtered data were included in the analysis.

Using a fitting function for the velocity profile that consists of a constant term, a quadratic term, and a growing and a decaying exponential term, a nonlinear regression analysis is employed to determine the values of two constants that minimize the least-squares error in the fit to the monotonically filtered μ-PIV data. Further details regarding this regression analysis are given by Damiano et al. (9). The variation, relative to a trial glycocalyx thickness, in the least-squares error, E, associated with the fit to the μ-PIV data tracks the quality of the fit relative to each trial thickness. The minimum in this variation in E corresponds to the best fit of all trials and provides our estimate for the hydrodynamically relevant glycocalyx thickness. Defining a normalized least-squares error, $E^* = E/E_{min}$, where E_{min} is the minimum value of E, our estimate of the hydrodynamically relevant glycocalyx thickness corresponds to the trial thickness associated with $E^* = 1$.

In the analysis of the μ-PIV data presented here, flow through the glycocalyx is assumed to be negligible and the no-slip condition is applied at the blood–glycocalyx interface, $r = a$. This assumption results in a lower-bound estimate of the hydrodynamically relevant glycocalyx thickness, as a permeable layer would provide less resistance and therefore need to be thicker than an impermeable layer to provide the same observed hydrodynamic drag on the recorded microspheres (8,9).

Statistical analysis

Data are expressed as mean ± one standard deviation (SD). Statistical significance between groups was determined using a two-tailed independent t-test. An experimental condition resulted in a hydrodynamically relevant glycocalyx if a test of hypothesis showed that the mean layer thickness was $\gg 0$ μm with $p < 0.05$.

RESULTS

Fig. 1 shows an example of a full μ-PIV data set obtained from a 34.4-μm-diameter arteriole before filtering the data for monotonicity. It is evident from the distribution of μ-PIV data in this vessel that the velocity profile is essentially axisymmetric. By collecting data sufficiently far downstream from vessel bifurcations, branches, or other flow disturbances, we were able to ensure that axisymmetric velocity distributions were present in all of the vessels that we analyzed. Since rolling or adherent leukocytes would break this symmetry, μ-PIV data were collected only when none were present within the field of view. The P-selectin antibody helped systemically reduce leukocyte rolling and adhesion.

An example result of microviscometric analysis applied to μ-PIV data obtained from a 42.1-μm-diameter arteriole soon after peak systole is shown in Fig. 2. At this time point in the cycle, the minimum associated with the least-squares error, E, in the fit to the μ-PIV data in this arteriole (i.e., when $E^* = 1$) corresponds to a hydrodynamically relevant thickness of the glycocalyx of 0.43 μm. By contrast, Fig. 3 shows an example where the hydrodynamically relevant glycocalyx is completely degraded in a 29.7-μm-diameter arteriole after systemic treatment with hyaluronidase.

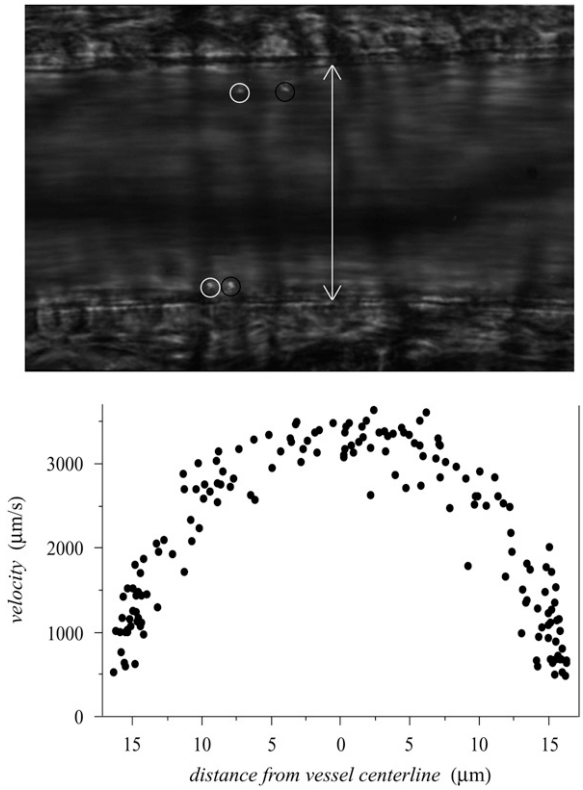

FIGURE 1 Typical bright-field image (*top*) showing dual images of two microspheres (~0.5-μm diameter) in a 46-μm-diameter mouse cremaster muscle arteriole in vivo. The dual images of each microsphere (*encircled* in white upstream and black downstream) are separated in time by the double flash interval, which was 9 ms for this data set. The white arrow indicates the anatomical diameter of the microvessel. Shown in the bottom panel is an unfiltered μ-PIV data set from a 34-μm-diameter arteriole. Note the axisymmetric distribution of the data. These data were folded onto one-half of the vessel diameter and monotonically filtered. This filtered subset of the data was then used in the nonlinear regression analysis to find the velocity profile, which can be seen, together with the monotonically filtered data, in row *C* of Fig. 5.

Estimated mean glycocalyx thickness in arterioles

Microviscometric analysis of our μ-PIV data, similar to those shown in Figs. 2 and 3 (see also Supplementary Material, Data S1), consistently revealed the presence of a hydrodynamically relevant surface glycocalyx in all of the arterioles that we examined before enzyme treatment with hyaluronidase. In arterioles ~20–70 μm in diameter (39.3 $\pm$ 8.8 μm, 23.3–61.2 μm, $n = 20$), the mean hydrodynamically relevant glycocalyx thickness was estimated to be 0.38 $\pm$ 0.11 μm (0.15–0.61 μm) as compared with 0.51 $\pm$ 0.15 μm (0.26–0.75 μm) found previously (11) in venules ~20–70 μm in diameter (40.9 $\pm$ 14.6 μm, 25.9–63.6 μm, $n = 9$). This difference was found to be statistically significant. The mean hydrodynamically relevant glycocalyx thickness after hyaluronidase treatment to degrade the layer in both arterioles and venules (11) was found not to be significantly different from zero (0.03 $\pm$ 0.04 μm, 0.00–0.11 μm in venules; 0.01 $\pm$ 0.02 μm, 0.00–0.07 μm in arterioles). These results are summarized in Fig. 4. Note that when the analysis is performed, assuming a permeable glycocalyx modeled as a Brinkman medium (8,9), results obtained are insensitive to the value of K, the hydraulic resistivity of the glycocalyx, for $K > \sim 10^9$ dyn-s/cm^4. This insensitivity to K is consistent with results found in venules before and after light-dye treatment to degrade the glycocalyx (9).

Influence of hemodynamic parameters on mean glycocalyx thickness

In a subset of the arterioles studied ($n = 8$), μ-PIV data were collected at four time points in the cardiac cycle. Example results from one such case are shown in Figs. 5 and 6 (see also Data S1). There was no statistically significant difference in the mean hydrodynamically relevant glycocalyx thickness between any two of the four different time points in the cardiac cycle (see Fig. 7). Furthermore, there appeared to be essentially no correlation between the hydrodynamically relevant glycocalyx thickness and either the centerline velocity (correlation coefficient, $\varrho = -0.12$), the centerline viscosity ($\varrho = 0.23$), the interfacial shear rate ($\varrho = -0.10$), or the interfacial shear stress ($\varrho = 0.09$). In addition to the lack of correlation with hemodynamic parameters, we found virtually no correlation between the hydrodynamically relevant glycocalyx thickness and the vessel diameter in either venules ($\varrho = 0.25$) or arterioles ($\varrho = -0.18$) ~20–70 μm in diameter.

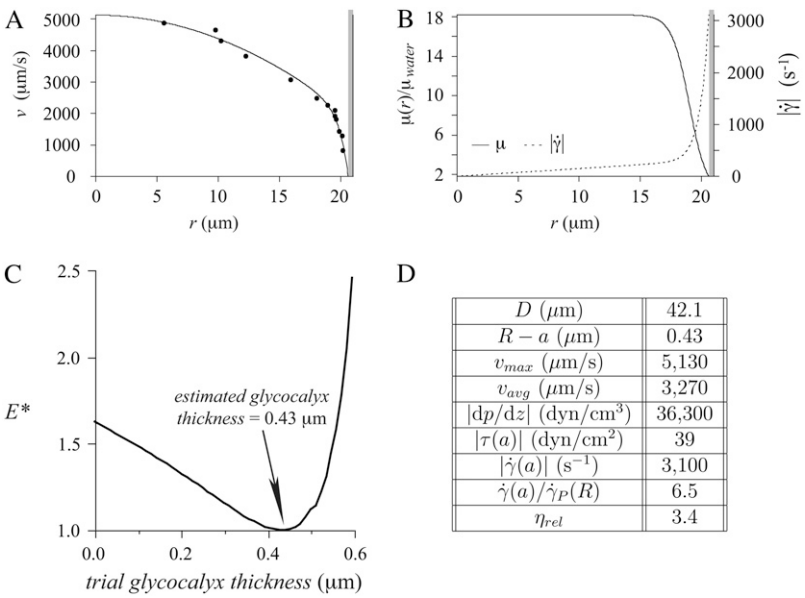

D (μm)	42.1
$R-a$ (μm)	0.43
v_{max} (μm/s)	5,130
v_{avg} (μm/s)	3,270
$\lvert dp/dz\rvert$ (dyn/cm^3)	36,300
$\lvert\tau(a)\rvert$ (dyn/cm^2)	39
$\lvert\dot{\gamma}(a)\rvert$ (s^{-1})	3,100
$\dot{\gamma}(a)/\dot{\gamma}_P(R)$	6.5
η_{rel}	3.4

FIGURE 2 Results from a 42.1-μm-diameter arteriole under control conditions in the mouse cremaster muscle. Shown in panel *A* are intravital fluorescent μ-PIV data (*symbols*) collected at the same time point in the cardiac cycle, and the corresponding predicted axisymmetric velocity profile extracted from the data (*curve*). Blood viscosity (*solid curve*) and shear-rate (*dashed curve*) profiles are shown in panel *B*. The shaded region near the vessel wall represents the endothelial glycocalyx. Shown in panel *C* is the variation, relative to trial glycocalyx thicknesses, in the normalized least-squares error, E^*, associated with the fit to the μ-PIV data shown in *A*. The estimated hydrodynamically effective thickness of the glycocalyx corresponds to the value of $R-a$ associated with the local minimum in this curve, which occurs at 0.43 μm in this case. Tabulated in panel *D* are the measured vessel diameter, D, the estimated glycocalyx thickness, $R-a$ (where $R=D/2$ is the vessel radius and a is the radial position of the blood–glycocalyx interface), the maximum, v_{max}, and average v_{avg}, velocities of the predicted axisymmetric velocity profile, the magnitude of the predicted axial pressure gradient, $|dp/dz|$, the magnitude of the predicted shear stress, $|\tau(a)|$, and the magnitude of the shear rate, $|\dot{\gamma}(a)|$, at the blood–glycocalyx interface, the ratio of the predicted interfacial shear rate, $\dot{\gamma}(a)$, to the wall shear rate, $\dot{\gamma}_P(R)$, of a Poiseuille flow having a centerline velocity equal to v_{max}, and the predicted relative apparent viscosity, η_{rel}.

Due to the finite time required to acquire the μ-PIV data ($\sim$15 min total for all four time points chosen within the cardiac cycle), it was possible that the prevailing flow conditions drifted somewhat during data collection. In an attempt to quantify these changes, the first and last data sets (A and A′) in each vessel were collected at the same time point in the cardiac cycle. Differences between the estimated distributions in velocity, viscosity, shear rate, or shear stress found at A and A′ would suggest that the overall flow conditions changed during the period of data acquisition. On average, the predicted centerline velocity, v_{max}, the interfacial shear rate, $\dot{\gamma}(\alpha)$, and the interfacial fluid shear stress, $\tau(\alpha)$, varied by $\sim$30% between A and A′, whereas the maximum variation in these quantities throughout the cardiac cycle averaged $\sim$50% for v_{max} and $\sim$80% for $\dot{\gamma}(\alpha)$ and $\tau(\alpha)$. Thus any drift in the overall flow conditions during the finite time required to collect the data was, on average, smaller than were the pulsatile changes in the flow observed throughout the cardiac cycle. Any drift in overall flow conditions is attributable to changes in hemodynamics upstream or downstream from the point of data collection, including changes in flow rate, vasomotor tone, and feed hematocrit.

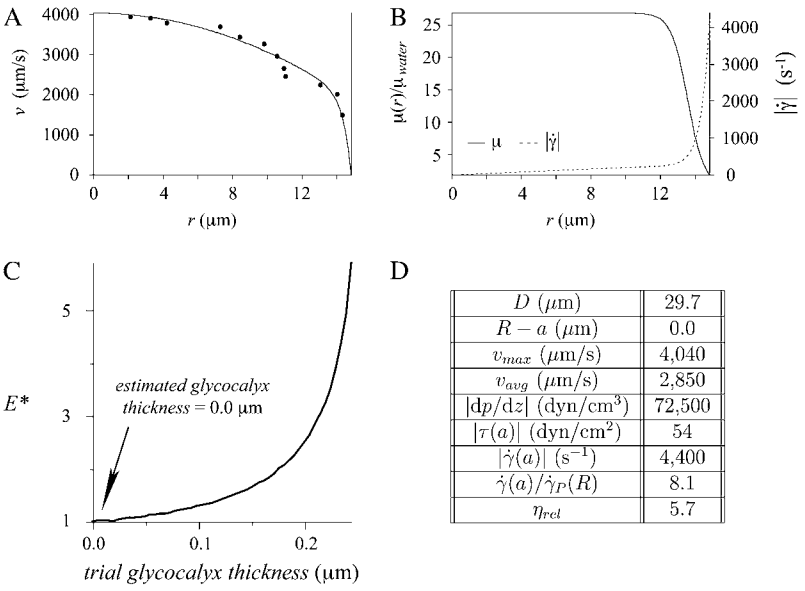

D (μm)	29.7
$R-a$ (μm)	0.0
v_{max} (μm/s)	4,040
v_{avg} (μm/s)	2,850
$\lvert dp/dz\rvert$ (dyn/cm^3)	72,500
$\lvert\tau(a)\rvert$ (dyn/cm^2)	54
$\lvert\dot{\gamma}(a)\rvert$ (s^{-1})	4,400
$\dot{\gamma}(a)/\dot{\gamma}_P(R)$	8.1
η_{rel}	5.7

FIGURE 3 Results from a 29.7-μm-diameter arteriole in the mouse cremaster muscle with the same interpretation as in Fig. 2, except after systemic hyaluronidase treatment. Note that in this arteriole, no hydrodynamically relevant glycocalyx remains after enzymatic degradation with hyaluronidase.

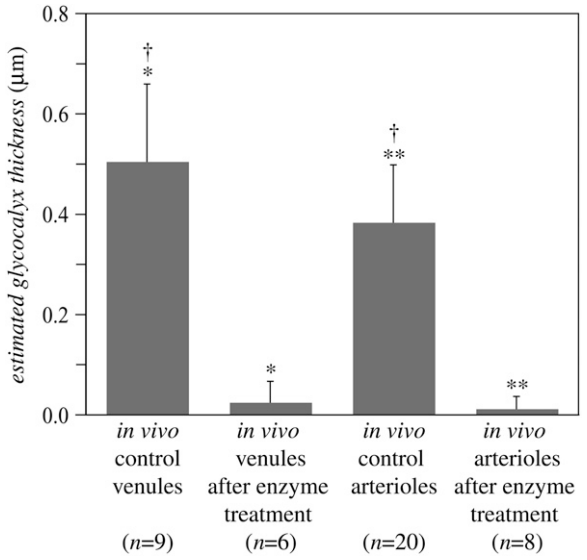

FIGURE 4 Hydrodynamically relevant glycocalyx thickness (mean and SD) as determined by microviscometric analysis in venules and arterioles in vivo, before and after treatment with hyaluronidase. Experiments were performed with 15 wild-type mice in venules and arterioles (20–70 μm in diameter). The mean hydrodynamically relevant glycocalyx thickness was found to be 0.51 ± 0.15 μm in control venules ($n = 9$) and 0.38 ± 0.11 μm in control arterioles ($n = 20$). The mean hydrodynamically relevant glycocalyx thickness after hyaluronidase treatment was found not to be significantly different from zero in either venules or arterioles. Symbols denote a significant difference via a nondirectional t-test ($p < 0.05$). Note the significant difference between the glycocalyx thickness in venules and arterioles in vivo.

DISCUSSION

These results provide the first direct in vivo evidence for the existence of a hydrodynamically relevant glycocalyx in arterioles >15 μm in diameter. While the mean layer thickness found is 5–10-fold greater than most images of the structure obtained using electron microscopy (18,19), at ~0.4 μm, it is nevertheless statistically significantly thinner than the mean hydrodynamically relevant glycocalyx thickness observed in similarly sized venules from the same tissue. A difference in mean glycocalyx thickness between venules and arterioles of ~0.1 μm may indeed be within the resolution of microviscometry. If one assumes that the hydrodynamically relevant glycocalyx is completely degraded after hyaluronidase treatment, then the positive mean layer thickness found in venules and arterioles after enzymatic degradation (~0.02 μm) could be regarded as a measure of the resolution inherent to the method's ability to estimate mean layer thickness. If this is true, then a difference of 0.1 μm in the mean hydrodynamically relevant glycocalyx thickness between venules and arterioles should be detectable using this approach.

This difference in mean hydrodynamically relevant glycocalyx thickness between venules and arterioles could be attributable to hemodynamic differences between these vessels. However, as well as there being essentially no correlation between the hydrodynamically relevant glycocalyx thickness and either the centerline velocity, v_{max}, the centerline viscosity, μ_{max}, the interfacial shear rate, $\dot{\gamma}(a)$, or the interfacial shear stress, $\tau(a)$, our results show there to be no statistically significant difference in any of these hemodynamic quantities between the population of arterioles and the population of venules (11) considered in Fig. 4. Furthermore, despite the fact that each of the above-referenced hemodynamic quantities varies considerably throughout the cardiac cycle (typically by ~50–80%), we found no statistically significant difference in the mean hydrodynamically relevant glycocalyx thickness between any two time points in the cardiac cycle. Collectively, these results suggest that the hemodynamic environment is not a strong determinant of the mean glycocalyx thickness. Thus, there may be a phenotypical difference between arteriolar and venular endothelium that might influence regulation of the glycocalyx and explain the difference observed between the mean hydrodynamically relevant glycocalyx thickness in arterioles and venules.

The fact that in all of the control arterioles that we observed, microviscometry revealed a hydrodynamically relevant glycocalyx, which was typically ~0.4 μm thick throughout the cardiac cycle, implies a vanishingly small fluid shear stress and fluid shear rate on the luminal surface of arteriolar endothelial cells. This was first illustrated experimentally by Smith et al. (8) using μ-PIV limited to particle tracers in the plasma-rich region near the vessel wall in postcapillary venules. They showed that a linear fit to these μ-PIV data consistently revealed a negative velocity when this line was extrapolated to the vessel wall, and concluded that, to satisfy the no-slip condition on the luminal endothelial-cell surface, a strongly exponential rather than linear velocity distribution must exist within the glycocalyx itself. This exponential behavior is consistent with the velocity profile that would arise through a porous material, such as a Brinkman medium (1,13,20–23). Damiano et al. (9) subsequently showed, using full-field μ-PIV data collected over the entire cross section of postcapillary venules, that microviscometric analysis (as was used in this study) provided an improved estimate of the hydrodynamically relevant glycocalyx thickness in venules, since it relaxed the requirement of a linear velocity distribution throughout the plasma-rich region near the vessel wall. The proposed exponential velocity distribution across the glycocalyx corresponds to a heavily retarded flow of plasma throughout glycocalyx, particularly near the luminal endothelial-cell surface. Thus, on the basis of our results, endothelial cells in arterioles, like venules, are essentially bathed in a quiescent fluid that does not circulate or turn over throughout the cardiac cycle. Convection is absent and transport of small molecules is diffusion-limited. The fluid shear rate, and as a consequence, the fluid shear stress, vanish on the luminal endothelial-cell surface. Thus, the fluid shear stress from the prevailing flow in the vessel lumen is transferred in the form of mechanical stress to the solid matrix components of the glycocalyx (20). This stress

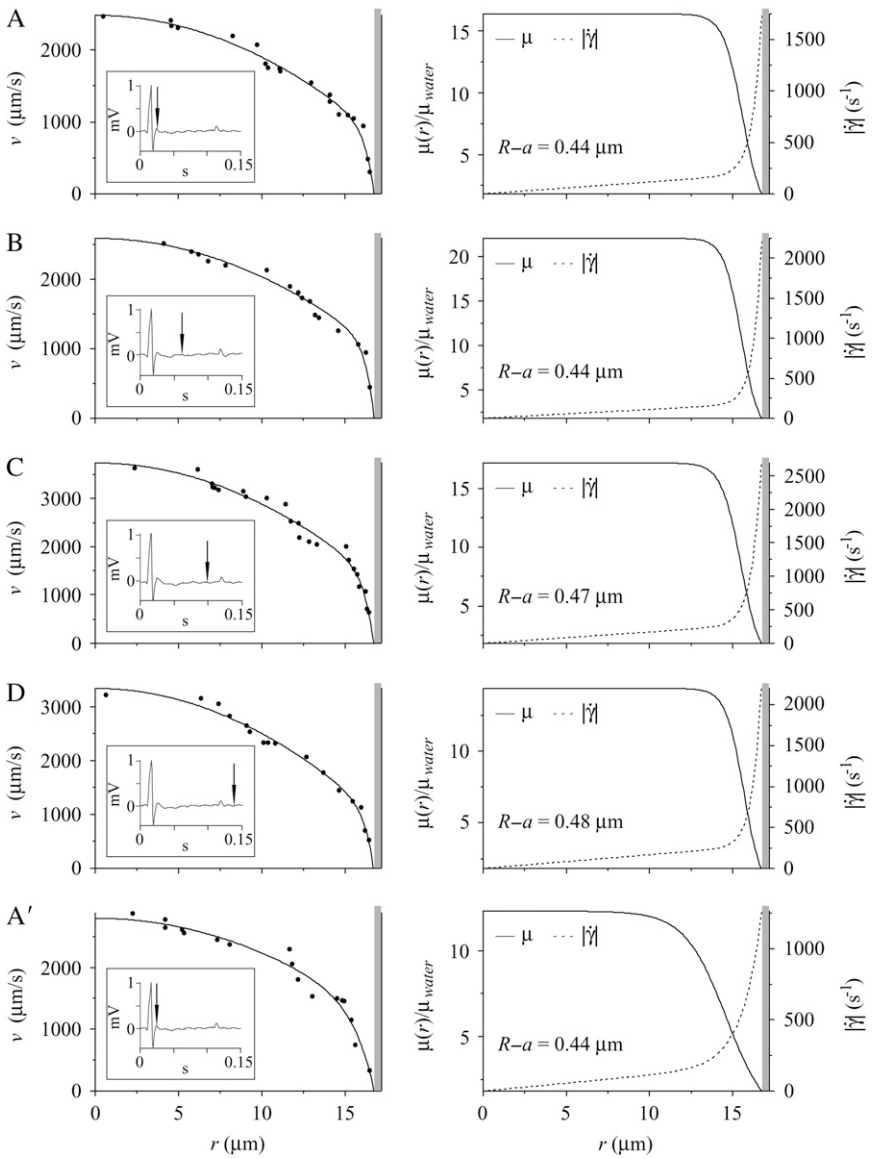

FIGURE 5 Results from a 34.4-μm-diameter arteriole under control conditions in the mouse cremaster muscle at four time points in the cardiac cycle. Shown in the left column are intravital fluorescent μ-PIV data (*symbols*) and the corresponding predicted axisymmetric velocity profiles (*curves*) extracted from the data. The inset shows the time point in the cardiac cycle where the data were collected (*vertical arrow*). Data sets A and A′ were collected 0.01 s after peak systole. Data sets B, C, and D, were respectively collected at 0.048, 0.085, and 0.123 s after peak systole. The five data sets were collected over a period of ~15 min, with set A being collected first and set A′ being collected last. Over this period, the heart rate of the mouse was ~400 BPM. Shown in the right column are the corresponding predicted blood viscosity profiles over the arteriolar cross section. Shown in the right column are the corresponding predicted blood-viscosity (*solid curve*) and shear-rate (*dashed curve*) distributions over the arteriolar cross section. The shaded region near the vessel wall represents the endothelial glycocalyx. The estimated glycocalyx thickness, $R - a$, is displayed for each of the five data sets. Notice that throughout the cardiac cycle there is little change in the thickness of the glycocalyx. Also note that the maximum observed centerline velocity occurs in data set C, and is ~50% greater than the centerline velocity observed in data set A.

in the solid components of the glycocalyx can be readily transferred, through transmembrane domains of core proteins in the glycocalyx, to the endothelial-cell cytoskeleton (8,24).

This revised perspective on our understanding of the mechanism for stress transmission to vascular endothelium, which was postulated on theoretical grounds by Damiano et al. (20) and later supported experimentally in venules by Smith et al. (8) and in arterioles by this study, certainly has important implications for endothelial-cell mechanotransduction and atherosclerosis. Even before this in vivo confirmation in arterioles was made, the role of the glycocalyx in endothelial-cell mechanotransduction was the focus of a variety of recent studies (3,4,24–26). In each of these studies, it was tacitly assumed that the in vivo results previously reported on the glycocalyx in capillaries and venules extended to arterioles. However, if further such studies are to be pursued, it is essential that the in vivo results of this study be reported, particularly since physiological and pathophysiological processes that are preferential to arterioles might be determinants or consequences of the state of the glycocalyx on arteriolar endothelium.

Our hemodynamic results for v_{avg} and v_{max} in control arterioles (Arterioles 1–11, 19-A−26-A, and 27; see Table S1 in Data S1) were in good agreement with the results of Tangelder et al. (14) in terms of v_{max} as well as the ratio v_{max}/v_{avg}, which we found, respectively, to be 4230 ± 3190 μm/s (1320–14,500 μm/s) and 1.58 ± 0.05 (1.52–1.70) for 20 arterioles (39.3 ± 8.7 μm diameter), and found to be 4026 ± 3437 μm/s (1290–14,400 μm/s) and 1.48 ± 0.05 for 12 arterioles (25.4 ± 4.2 μm diameter). Thus, the prevailing flow conditions in both studies were remarkably similar as measured by centerline velocity and bluntness of the velocity profile. The slightly higher ratio of v_{max}/v_{avg} that we found is

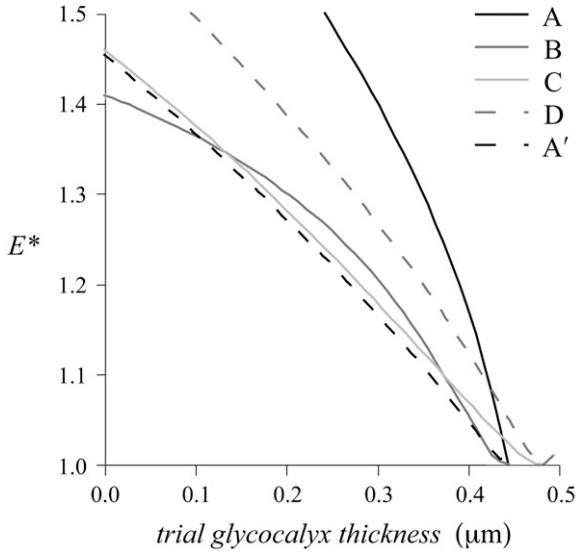

$D = 34.4\ \mu$m	A	B	C	D	A′
$R - a$ (μm)	0.44	0.44	0.47	0.48	0.44
v_{max} (μm/s)	2,480	2,580	3,740	3,340	2,790
v_{avg} (μm/s)	1,530	1,660	2,320	1,990	1,760
$\lvert dp/dz \rvert$ (dyn/cm^3)	24,900	32,000	38,400	31,300	18,000
$\lvert\tau(a)\rvert$ (dyn/cm^2)	22	28	34	28	16
$\lvert\dot{\gamma}(a)\rvert$ (s^{-1})	1,700	2,200	2,700	2,200	1,300
$\dot{\gamma}(a)/\dot{\gamma}_P(R)$	6.2	7.7	6.4	5.8	4.0
η_{rel}	3.0	3.2	2.9	2.8	2.4

FIGURE 6 The variation, relative to trial glycocalyx thicknesses, in the normalized least-squares error, E^*, associated with the fit to the μ-PIV data for each of the five data sets shown in Fig. 5. Tabulated below is the diameter, $D = 2R$, of the arteriole and the estimated glycocalyx thickness, $R - a$, associated with each data set, as well as the corresponding values of the same hemodynamic parameters shown in Figs. 2 and 3.

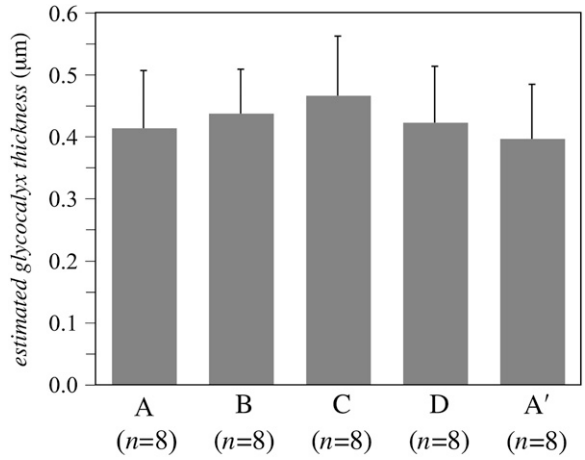

FIGURE 7 Hydrodynamically relevant glycocalyx thickness (mean and SD) as determined by microviscometric analysis in arterioles in vivo at four time points in the cardiac cycle ($n = 8$). Experiments were performed in arterioles (20–70 μm in diameter) of five wild-type mice. The mean hydrodynamically relevant glycocalyx thickness was found to be 0.42 $\pm$ 0.09 μm at point A, 0.44 $\pm$ 0.07 μm at point B, 0.47 $\pm$ 0.10 μm at point C, 0.42 $\pm$ 0.09 μm at point D, and 0.40 $\pm$ 0.09 μm at point A′. These differences were found not to be statistically significant ($p > 0.2$).

likely due to the larger diameters of the arterioles that we considered. As the vessel diameter increases, the blunting of the velocity profile decreases (i.e., the Fåhræus effect diminishes) and this ratio approaches 2, even for blood (27,28).

However, important differences exist between the two studies, which render the approach taken by Tangelder et al. (14) unable to accurately resolve the velocity distribution in the plasma-rich region near the vessel wall, and therefore unable to estimate or even detect the endothelial glycocalyx. In particular, Tangelder et al. (14) used irregularly-shaped, fluorescently-labeled platelets (nominally $\sim$2 μm in diameter) for particle tracers in their study, whereas we used regularly-shaped $\sim$0.5-μm-diameter fluorescent polystyrene microspheres. Inspection of the viscosity profiles obtained (see Figs. 2 and 3 and figures in Data S1) reveal that the plasma-rich region typically extends $\sim$3–5 μm from the vessel wall (of which $\sim$0.5 μm is occupied by the glycocalyx). Given the large variation in velocity that occurs over the length scale of a platelet within this plasma-rich zone, these particle tracers are ultimately too large to provide sufficient spatial resolution necessary to accurately extract the velocity and shear rate profiles near the vessel wall. Consequently, evidence requiring the existence of a highly nonlinear velocity profile through the glycocalyx to satisfy the no-slip condition on the endothelial-cell surface was not apparent from the data of Tangelder et al. (14). On the other hand, for the range of vessel diameters that they considered, platelets are sufficiently small to provide the resolution necessary to accurately estimate the centerline velocity. In addition, since the average velocity is obtained from integration of the estimated velocity profile, errors in their profiles near the vessel wall were diminished when these distributions were integrated to compute v_{avg}. Thus, it is not surprising that v_{max} and v_{max}/v_{avg} reported above for this study and for Tangelder et al. (14) were in good agreement despite the inherent differences in these two approaches.

CONCLUSION

This study provides the first direct in vivo demonstration of a hydrodynamically relevant endothelial glycocalyx in arterioles and a vanishingly small fluid shear stress on arteriolar endothelium throughout the cardiac cycle, which, until now, has only been established for steady flow in venules. This fundamental result impacts our understanding of the biophysics of signal-transduction and biomolecular-transport processes that might be preferential to arterioles and is a prerequisite to studies that have speculated on the existence of a hydrodynamically relevant glycocalyx in arterioles based on extrapolation from previous results in venules. Similar experimental methods to those employed here, using microviscometric analysis in the unsteady flow regimes of arterioles, can now be applied to functionally interrogate the endothelial glycocalyx in future studies involving microvascular permeability, endothelial-cell mechanotransduction,

and vascular disease states associated with inflammation and atherosclerosis.

SUPPLEMENTARY MATERIAL

To view all of the supplemental files associated with this article, visit www.biophysj.org.

We thank J. Jiang for providing laboratory and surgical assistance, D. R. Potter for assistance with software and instrumentation, and B. P. Helmke for helpful discussions.

This work was supported by the National Institutes of Health grants No. HL 076499 and HL 082870.

REFERENCES

1. Weinbaum, S., J. M. Tarbell, and E. R. Damiano. 2007. The structure and function of the endothelial glycocalyx layer. *Annu. Rev. Biomed. Eng.* 9:121–167.
2. Nieuwdorp, M., H. L. Mooij, J. Kroon, B. Atasever, J. A. E. Spaan, C. Ince, F. Holleman, M. Diamant, R. J. Heine, J. B. L. Hoekstra, J. J. P. Kastelein, E. S. G. Stroes, and H. Vink. 2006. Endothelial glycocalyx damage coincides with microalbuminuria in type 1 diabetes. *Diabetes.* 55:1127–1132.
3. Florian, J. A., J. R. Kosky, K. Ainslie, Z. Pang, R. O. Dull, and J. M. Tarbell. 2003. Heparan sulfate proteoglycan is a mechanosensor on endothelial cells. *Circ. Res.* 93:e136–e142.
4. Yao, Y., A. Rabodzey, and C. F. Dewey. 2007. Glycocalyx modulates the motility and proliferative response of vascular endothelium to fluid shear stress. *Am. J. Physiol.* 293:H1023–H1030.
5. Vink, H., and B. R. Duling. 1996. Identification of distinct luminal domains for macromolecules, erythrocytes, and leukocytes within mammalian capillaries. *Circ. Res.* 79:581–589.
6. Henry, C. B., and B. R. Duling. 1999. Permeation of the luminal capillary glycocalyx is determined by hyaluronan. *Am. J. Physiol.* 277:H508–H514.
7. Henry, C. B., and B. R. Duling. 2000. TNF-α increases entry of macromolecules into luminal endothelial cell glycocalyx. *Am. J. Physiol.* 279:H2815–H2823.
8. Smith, M. L., D. S. Long, E. R. Damiano, and K. Ley. 2003. Near-wall micro-PIV reveals a hydrodynamically relevant endothelial surface layer in venules in vivo. *Biophys. J.* 85:637–645.
9. Damiano, E. R., D. S. Long, and M. L. Smith. 2004. Estimation of viscosity profiles using velocimetry data from parallel flows of linearly viscous: application to microvascular hemodynamics. *J. Fluid Mech.* 512:1–19.
10. Long, D. S., M. L. Smith, A. R. Pries, K. Ley, and E. R. Damiano. 2004. Microviscometry reveals reduced blood viscosity and altered shear rate and shear stress profiles in microvessels after hemodilution. *Proc. Natl. Acad. Sci. USA.* 101:10060–10065.
11. Potter, D. R., and E. R. Damiano. 2008. The hydrodynamically relevant endothelial-cell glycocalyx observed in vivo is absent in vitro. *Circ. Res.* 102:770–776.
12. Cokelet, G. 1999. Viscometric, in vitro and in vivo blood viscosity relationships: how are they related? *Biorheology.* 36:343–358.
13. Damiano, E. R., D. S. Long, F. H. El-Khatib, and T. M. Stace. 2004. On the motion of a sphere in a Stokes flow parallel to a Brinkman half-space. *J. Fluid Mech.* 500:75–101.
14. Tangelder, G. J., D. W. Slaaf, A. M. Muijtjens, T. Arts, M. G. Oude Egbrink, and R. S. Reneman. 1986. Velocity profiles of blood platelets and red blood cells flowing in arterioles of the rabbit mesentery. *Circ. Res.* 59:505–514.
15. Tangelder, G. J., D. W. Slaaf, T. Arts, and R. S. Reneman. 1988. Wall shear rate in arterioles in vivo: least estimates from platelet velocity profiles. *Am. J. Physiol.* 254:H1059–H1064.
16. Ley, K., D. C. Bullard, M. L. Arbonés, R. Bosse, D. Vestweber, T. F. Tedder, and A. L. Beaudet. 1995. Sequential contribution of L- and P-selectin to leukocyte rolling in vivo. *J. Exp. Med.* 181:669–675.
17. Gretz, J. E., and B. R. Duling. 1995. Measurement uncertainties associated with the use of bright-field and fluorescence microscopy in the microcirculation. *Microvasc. Res.* 49:134–140.
18. Haldenby, K. A., D. C. Chappell, C. P. Winlove, K. H. Parker, and J. A. Firth. 1994. Focal and regional variations in the composition of the glycocalyx of large vessel endothelium. *J. Vasc. Res.* 31:2–9.
19. Sims, D. E., and M. M. Horne. 1994. Non-aqueous fixative preserves macromolecules on the endothelial cell surface: an in situ study. *Eur. J. Morphol.* 32:59–64.
20. Damiano, E. R., B. R. Duling, K. Ley, and T. C. Skalak. 1996. Axisymmetric pressure-driven flow of rigid pellets through a cylindrical tube lined with a deformable porous wall layer. *J. Fluid Mech.* 314:163–189.
21. Damiano, E. R. 1998. The effect of the endothelial-cell glycocalyx on the motion of red blood cells through capillaries. *Microvasc. Res.* 55:77–91.
22. Secomb, T. W., R. Hsu, and A. R. Pries. 1998. A model for red blood cell motion in glycocalyx-lined capillaries. *Am. J. Physiol.* 274:H1016–H1022.
23. Feng, J., and S. Weinbaum. 2000. Lubrication theory in highly compressible porous media: the mechanics of skiing, from red cells to humans. *J. Fluid Mech.* 422:281–317.
24. Weinbaum, S., X. Zhang, Y. Han, H. Vink, and S. C. Cowin. 2003. Mechanotransduction and flow across the endothelial glycocalyx. *Proc. Natl. Acad. Sci. USA.* 100:7988–7995.
25. Tarbell, J. M., and M. Y. Pahakis. 2006. Mechanotransduction and the glycocalyx. *J. Intern. Med.* 259:339–350.
26. Jacob, M., M. Rehm, M. Loetsch, J. O. Paul, D. Bruegger, U. Welsch, P. Conzen, and B. F. Becker. 2007. The endothelial glycocalyx prefers albumin for evoking shear stress-induced, nitric oxide-mediated coronary dilatation. *J. Vasc. Res.* 44:435–443.
27. Poiseuille, J. L. M. 1830. Research on the causes of movement of blood in the veins. *J. Physiol. Exp. Pathol.* 10:277–295.
28. Fåhræus, R. 1928. The flow conditions and distribution of blood cells in the vascular system. *Klin. Wochenschr.* 7:100–106.